

# Topological magnons in a non-coplanar magnetic order on the triangular lattice

Linli Bai<sup>1,2</sup>, Ken Chen<sup>1,2,\*</sup>

<sup>1</sup> School of Physical Science and Technology & Key Laboratory for Magnetism and Magnetic Materials of the MoE, Lanzhou University, Lanzhou 730000, China

<sup>2</sup> Lanzhou Center for Theoretical Physics, Key Laboratory of Theoretical Physics of Gansu Province, & Key Laboratory of Quantum Theory and Applications of MoE, Lanzhou University, Lanzhou, Gansu 730000, China

\*Corresponding author E-mail: chen20@lzu.edu.cn

## Abstract

The bond-dependent Kitaev interaction  $K$  is familiar in the effective spin model of transition metal compounds with octahedral ligands. In this work, we find a peculiar non-coplanar magnetic order can be formed with the help of  $K$  and next-nearest neighbor Heisenberg coupling  $J_2$  on the triangular lattice. It can be seen as a miniature version of skyrmion crystal, since it has nine spins and an integer topological number in a magnetic unit cell. The magnon excitations in such an order are studied by the linear spin-wave theory. Of note is that the change in the relative size of  $J_2$  and  $K$  produces topological magnon phase transitions although the topological number remains unchanged. We also calculated the experimentally observable thermal Hall conductivity, and found that the signs of thermal Hall conductivity will change with topological phase transitions or temperature changes in certain regions.

Keywords: non-coplanar magnetic order; topological magnons; thermal Hall effect.

## 1 Introduction

Magnon is the quantum of low-energy collective excitation in a magnetic system [1–3]. Since a magnon does not generate Joule heating during motion and has a much longer diffusion length than an electron [4–6], it has application prospects for storing and disseminating information in the future [6]. Inspired by topological insulators which can support chiral edge/surface states that are immune to backscattering [7, 8], researchers are also committed to find corresponding phenomena in magnons [9–18]. Topologically non-trivial magnons can be driven by a thermal gradient, forming transverse heat currents by the Berry phase mechanism [19]. This is called the thermal Hall effect [20–32], which has been experimentally observed in pyrochlore [21, 23] and kagome [11, 27] ferromagnets. Relevant research has been in full swing [29, 33].

The non-planar spin textures with non-zero topological numbers are also a key research focus in condensed matter physics [34–40], and the most representative one is the skyrmion [34, 35]. In the continuous limit, a skyrmion is topologically protected, which means it cannot be generated or removed by any continuous deformation [35]. In the actual magnetic system, although the lattice is discrete and the size of the skyrmion is limited, a skyrmion is still relatively stable, which allows it to be manipulated independently as a quasi-particle [41]. In recent years, researchers have begun to pay attention to the magnon excitations in the skyrmion [6]. The topological magnons in ferromagnetic and anti-ferromagnetic skyrmion crystals have been discovered [42–48], and the topological phase transitions caused by the interactions or magnetic field are discussed as well [44, 45]. However, as far as we know, in previous works, researchers mainly involved the skyrmions in non-centrosymmetric magnets which are formed with the help of chiral Dzyaloshinskii-Moriya interaction. This is just the tip of the iceberg of topological non-trivial spin textures [39]. On the one hand, it has been proved that the skyrmion can also appear in the centrosymmetric magnets as a result of other interactions [49–60], such as dipolar interaction [49, 50], the single-ion anisotropy [51–58] or the bond-dependent

interactions [54, 61]. On the other hand, beyond the skyrmion, there are many magnetic quasi-particles coming into the sight of researchers in recent years [39, 62, 63]. Whether topological magnons or relevant phase transitions exist within such spin textures remains to be further explored.

In this work, we study the interplay of Heisenberg and Kitaev interactions on the triangular lattice. The bond-dependent Kitaev interaction is widely considered in the theoretical model describing transition metal compounds with octahedral crystal field [64–66]. We find a peculiar non-coplanar magnetic order that can be formed by the competition between  $K$  and next nearest neighbor Heisenberg coupling  $J_2$ . There are nine spins in a magnetic unit cell and the topological number is  $\pm 1(\pm 2)$ , thus it can be seen as a miniature version of (high-Q) skyrmion crystal [67]. Then we focus on the magnon excitations in such order. Through the linear spin-wave theory, we calculate the Chern number of each magnon band, and based on this, different regions are distinguished. The change of  $J_2$  will produce topological phase transitions although the topological number in real space remains unchanged. Since thermal Hall conductivity is related to the magnon band topology [31], finally, we calculate the thermal Hall conductivity and discussed its distinctions in different areas. Thermal Hall conductivity is dominated by the Berry curvature in the lowest bands at low temperatures. We also found that in certain regions, the signs of thermal Hall conductivity will change with topological phase transitions or temperature changes.

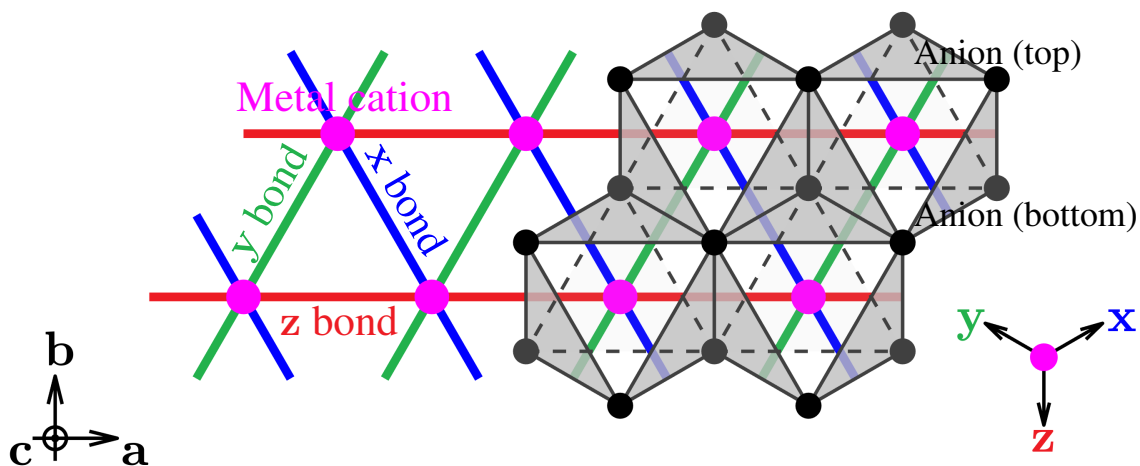


Figure 1: Schematic structure of the Kitaev directions in a triangular lattice. The Kitaev interaction appears along with an octahedral crystal field where the metal cations are located at the center of octahedral ligands [66, 68]. The global coordinate system  $\mathbf{a}$ - $\mathbf{b}$ - $\mathbf{c}$  is shown in the bottom left, where the triangular lattice composed of metal cations lies in the  $\mathbf{a}$ - $\mathbf{b}$  plane and  $\mathbf{c}$  is perpendicular to this plane. We mark the  $x$ ,  $y$ , and  $z$  bonds in blue, green, and red, respectively. In the  $\mathbf{a}$ - $\mathbf{b}$ - $\mathbf{c}$  coordinate system, their corresponding Kitaev directions are given by  $\mathbf{x} = [\sqrt{2}/2, \sqrt{6}/6, \sqrt{3}/3]$ ,  $\mathbf{y} = [-\sqrt{2}/2, \sqrt{6}/6, \sqrt{3}/3]$ ,  $\mathbf{z} = [0, -\sqrt{6}/3, \sqrt{3}/3]$ , respectively.

## 2 Model

We consider the following model on a triangular lattice,

$$\mathcal{H} = J_2 \sum_{\langle\langle ij \rangle\rangle} \mathbf{S}_i \cdot \mathbf{S}_j + K \sum_{\langle ij \rangle_\gamma} S_i^\gamma S_j^\gamma - \mathbf{h} \cdot \sum_i \mathbf{S}_i, \quad (1)$$

where  $J_2$  is the exchange parameter of the next-nearest neighbor Heisenberg coupling.  $\mathbf{S}_i$  represents the spin at site  $i$  and  $S_i^\gamma = \mathbf{S}_i \cdot \vec{\gamma}$ , where  $\vec{\gamma}$  is the bond-dependent Kitaev direction. For the three types of bonds  $x$ ,  $y$ , and  $z$ , as shown in Fig. 1,  $\vec{\gamma}$  corresponds to  $\mathbf{x}$ ,  $\mathbf{y}$ , and  $\mathbf{z}$ , respectively. The vectors  $\mathbf{x}$ ,  $\mathbf{y}$ , and  $\mathbf{z}$  are perpendicular to each other, forming a coordinate system  $\mathbf{x}$ - $\mathbf{y}$ - $\mathbf{z}$ .  $K$  is the exchange parameter of Kitaev interaction. In practical materials related to triangular lattices, the Kitaev interaction appears along with octahedral ligands [66, 68]. Accordingly, the Kitaev directions

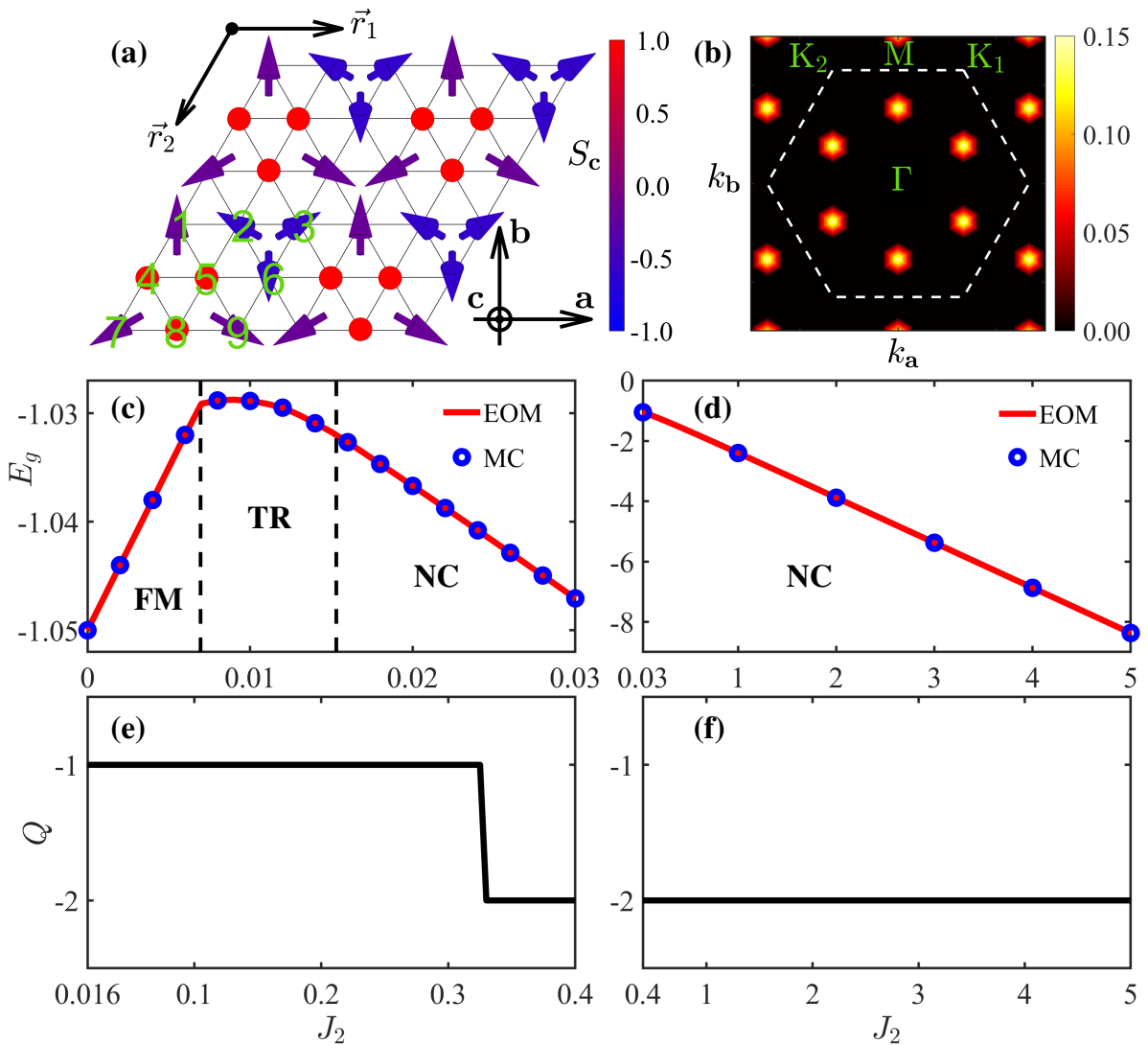


Figure 2: (a) Typical spin configuration of the non-coplanar order when  $K = -1$ ,  $J_2 = 1$ , and  $h = 0.05$ . The small arrows indicate directions of spins and their colors are based on the out of plane component. The magnetic unit cell includes nine spins. (b) The spin structure factor corresponds to (a), the peaks are located at the point of  $2\mathbf{M}/3$ . (c)-(d) The classic ground-state energy  $E_g$  as a function of  $J_2$  when  $K = -1$ ,  $h = 0.05$ . The result of energy optimization method (EOM) and Monte Carlo method is consistent. The ground state begins with the ferromagnetic (FM) order and rapidly transitions through a narrow transition region (TR) to the non-coplanar (NC) order. As  $J_2$  increases further, the ground state remains in non-coplanar order. (e)-(f) The topological number  $Q$  versus  $J_2$  in the non-coplanar order region. The topological number changes from  $-1$  to  $-2$  when  $J_2 \approx 0.326$ .

are fixed. To better illustrate them, we introduce a global coordinate system  $\mathbf{a-b-c}$ . In Fig. 1, the  $\mathbf{a-b-c}$  and the  $\mathbf{x-y-z}$  coordinate systems are shown on the bottom left and bottom right, respectively. The relationship between the  $\mathbf{x-y-z}$  and the  $\mathbf{a-b-c}$  coordinates systems satisfies

$$\begin{pmatrix} \mathbf{x} \\ \mathbf{y} \\ \mathbf{z} \end{pmatrix} = \begin{pmatrix} \frac{\sqrt{2}}{2} & \frac{\sqrt{6}}{6} & \frac{\sqrt{3}}{3} \\ -\frac{\sqrt{2}}{2} & \frac{\sqrt{6}}{6} & \frac{\sqrt{3}}{3} \\ 0 & -\frac{\sqrt{6}}{3} & \frac{\sqrt{3}}{3} \end{pmatrix} \begin{pmatrix} \mathbf{a} \\ \mathbf{b} \\ \mathbf{c} \end{pmatrix}. \quad (2)$$

The last term is the Zeeman term caused by a magnetic field  $\mathbf{h} = hc$ , which is perpendicular to the triangular lattice plane.

We use the parallel-tempering Monte Carlo simulations [69, 70] to uncover the spin textures. After Monte Carlo simulations, the classic ground state is then obtained by iteratively aligning the spins with their local fields [71]. Other numerical energy optimization methods are also used to check if

the energy is at a minimum. Then we use the ground-state energy as well as the spin structure factor  $\mathcal{S}_{\mathbf{k}} = \frac{1}{N_{total}^2} \left| \sum_i \mathbf{S}_i e^{-i\mathbf{k}\cdot\mathbf{R}_i} \right|^2$  [49, 72] to distinguish different phases. In the following, all the spin configurations are plotted in the **a-b-c** coordinate system.

### 3 The non-coplanar order

Through the above methods, we find a non-coplanar order can be stabilized by the competition between negative  $K$  and small positive  $J_2$ . We take a representative point ( $K = -1$ ,  $J_2 = 1$ ,  $h = 0.05$ ) as an example to illustrate its typical spin configuration in Fig.2 (a). The configuration has  $C_3$  rotational symmetry around the **c**-axis. There are nine spins in a magnetic unit cell ( $N = 9$ ) and the ordering wave vector is located at the  $2\mathbf{M}/3$  point, as shown in Fig.2 (b). Since the skyrmion crystal has an integer topological number in a magnetic unit cell, first, we calculate the solid angle  $\Omega_{\Delta}$  of each elementary triangle. In the discrete lattice, it can be obtained as [73]

$$\cos\left(\frac{\Omega_{\Delta}}{2}\right) = \frac{1 + \mathbf{S}_i \cdot \mathbf{S}_j + \mathbf{S}_i \cdot \mathbf{S}_k + \mathbf{S}_j \cdot \mathbf{S}_k}{\sqrt{2(1 + \mathbf{S}_i \mathbf{S}_j)(1 + \mathbf{S}_i \mathbf{S}_k)(1 + \mathbf{S}_j \mathbf{S}_k)}}, \quad (3)$$

where  $\mathbf{S}_i$  is the spin at site  $i$ . The sign of  $\Omega_{\Delta}$  is determined as  $\text{sign}(\Omega_{\Delta}) = \text{sign}[\mathbf{S}_i \cdot (\mathbf{S}_j \times \mathbf{S}_k)]$ . Note that on each triangle, the  $i$ ,  $j$ , and  $k$  are arranged counterclockwise. The topological number  $Q$  is the sum of solid angles in a magnetic unit cell,

$$Q = \frac{1}{4\pi} \sum_{\Delta} \Omega_{\Delta}. \quad (4)$$

The topological number  $Q$  of the non-coplanar order can be either  $\pm 1$  or  $\pm 2$  (for details, see the next paragraph), and the positive and negative signs can be selected by magnetic fields of different signs. The magnetic field is not the cause of the formation of this magnetic order, but it can eliminate the degeneracy when all spins are reversed.

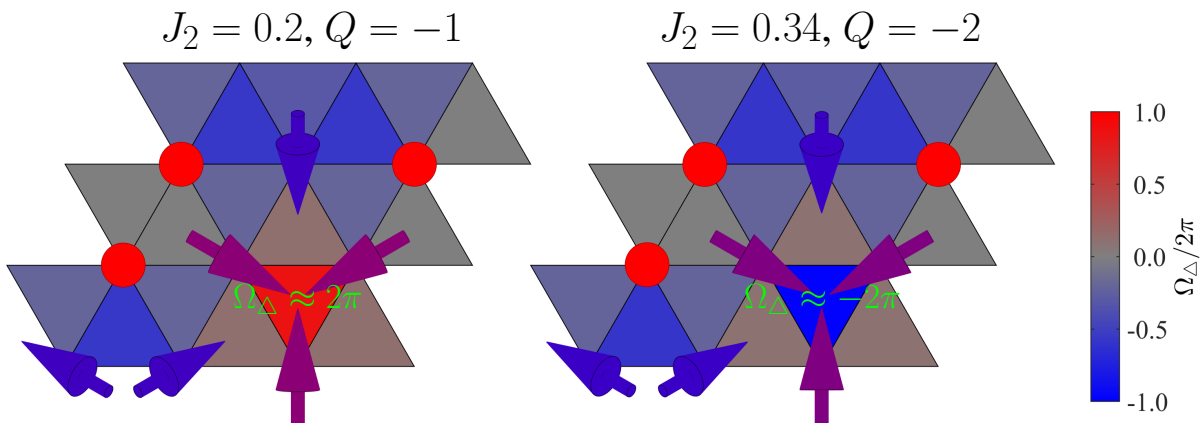


Figure 3: We compared the solid angle  $\Omega_{\Delta}$  distribution when topological number is -1 and -2. Three spins are almost in-plane and they have the same out of plane component  $S_c$ . As  $J_2$  increases, the  $S_c$  continuously changes from a small positive value to a small negative value, the solid angle formed by three spins changes as  $(< 2\pi) \rightarrow 2\pi \rightarrow -2\pi \rightarrow (> -2\pi)$ . Thus, the topological number (in unit of  $4\pi$ ) as the sum of solid angle reduce by 1.

Now we illustrate the influence of  $J_2$  interaction. The ground state of the pure Kitaev model is ferromagnetic order [74]. As shown in Fig. 2(c), after fixing  $K = -1$  and  $h = 0.05$ , a small  $J_2$  ( $\approx 0.016$ ) will induce the non-coplanar order. A narrow transition area has been identified before entering the non-coplanar order, and we omit its details. Next, we continue to increase  $J_2$ . As shown in Fig. 2(d), at least when  $J_2$  is less than 5, the non-coplanar order has always existed as the ground state. Of note is that the topological number will undergo a change as  $J_2$  increases. As shown in Fig. 2(e) and (f), when  $J_2 \in [0.016, 0.326]$  the topological number is  $-1$ , and it becomes  $-2$  when  $J_2$

is larger than 0.326. Since the energy and its derivatives are continuous at  $J_2 \approx 0.326$ , to understand what changes have occurred, we compared the solid angle distribution before and after such point. As shown in Fig. 3, the jump of topological numbers is due to the continuous variation of three almost in-plane spins. They have the same out of plane components  $S_c$ , and as  $S_c$  continuously changes from a small positive value to a small negative value, the solid angle formed by three spins will decrease by  $4\pi$ .

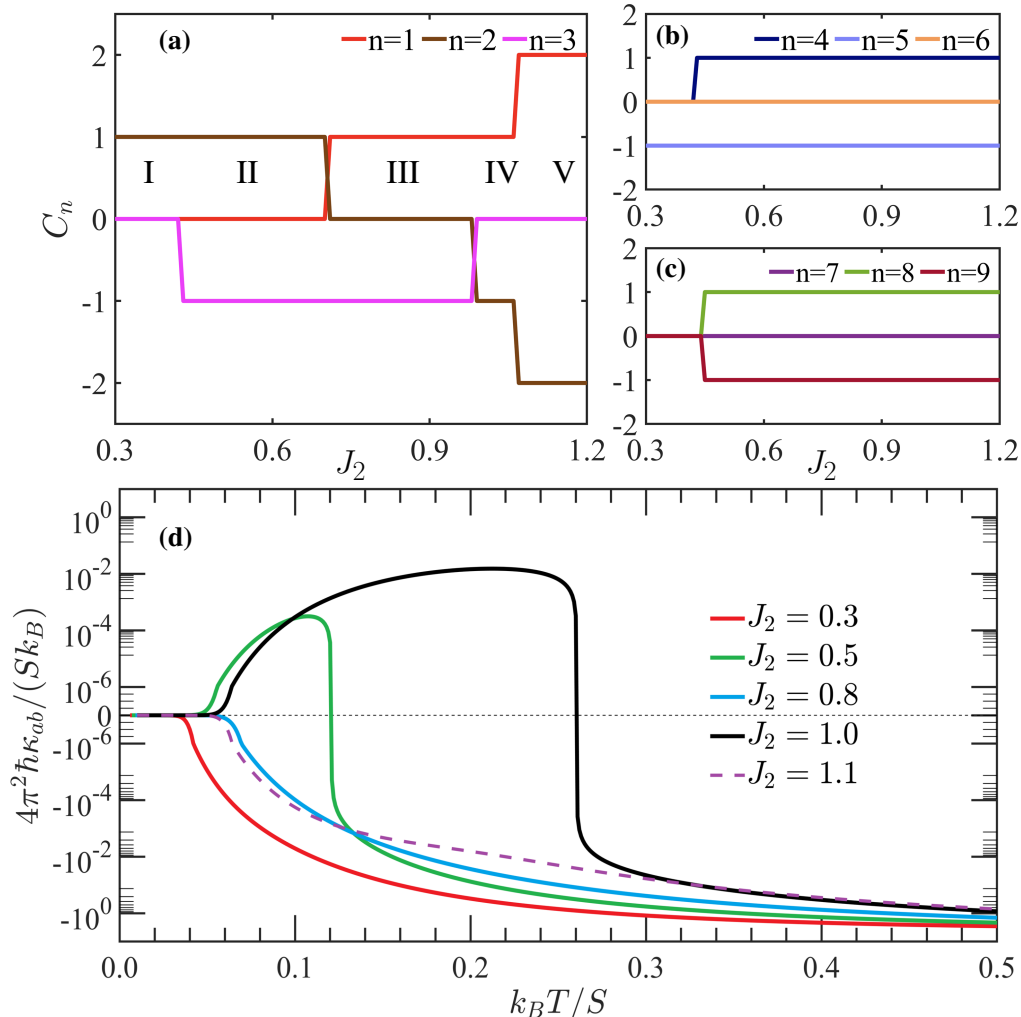


Figure 4: (a)-(c) Chern numbers as a function of  $J_2$ , and  $C_1, C_2, \dots, C_9$  correspond with the lowest to the highest band, respectively. Five areas are distinguished by different Chern numbers. We marked them with Roman numerals I-V in (a). (d) The magnon thermal Hall conductivity as a function of temperature for variant  $J_2$ , which belong to different areas in (a).

## 4 Topological magnon and thermal Hall effect

To consider magnon excitations in our non-coplanar order, we use the linear spin-wave theory. Its details can be found in Appendix. A. If a magnon band is separate from the upper and lower energy bands, we can capture its topological properties by calculating the Chern number. The Chern number of the band  $n$  ( $C_n$ ) is defined as the integral of the Berry curvature  $\Omega_{n,\mathbf{k}}$  over the first Brillouin zone (FBZ) of a magnetic unit cell

$$C_n = \frac{1}{2\pi} \int_{\text{FBZ}} \Omega_{n,\mathbf{k}} d^2\mathbf{k}. \quad (5)$$

The Berry curvature can be calculated as [30]

$$\Omega_{n,\mathbf{k}} = -2 \operatorname{Im} \sum_{\substack{m=1 \\ m \neq n}}^{2N} \frac{\left( GT_{\mathbf{k}}^\dagger \partial_a \mathcal{H}_{\mathbf{k}} T_{\mathbf{k}} \right)_{nm} \left( GT_{\mathbf{k}}^\dagger \partial_b \mathcal{H}_{\mathbf{k}} T_{\mathbf{k}} \right)_{mn}}{\left[ (G\mathcal{E}_{\mathbf{k}})_{nn} - (G\mathcal{E}_{\mathbf{k}})_{mm} \right]^2}, \quad (6)$$

where  $G$ ,  $\mathcal{H}_{\mathbf{k}}$ ,  $T_{\mathbf{k}}$  and  $\mathcal{E}_{\mathbf{k}}$  are all  $2N \times 2N$  matrices, and  $G$  is a diagonal matrix whose first  $N$  diagonal elements are 1, and the final  $N$  diagonal elements are  $-1$ . The definitions of the rest matrices are shown in Appendix. A.

In this section, we mainly focus on the impact of  $J_2$ , and consider a moderate parameter range  $J_2 \in [0.3, 1.2]$  since there are degeneracy points in the energy band when  $J_2$  is smaller. Fig. 4(a)-(c), show the variation of Chern number with  $J_2$  while fixing  $K = -1$ ,  $h = 0.05$ . The nonzero Chern numbers are widely present within the parameter range, indicating the existence of non-trivial band topology. The Chern number of the lowest three bands ( $C_1, C_2, C_3$ ) changes with the increase of  $J_2$  as  $(0, 1, 0) \rightarrow (0, 1, -1) \rightarrow (1, 0, -1) \rightarrow (1, -1, 0) \rightarrow (2, -2, 0)$ , sequentially. Five different areas are distinguished, and we marked them with Roman numerals I-V in Fig. 4(a). Specifically, the real space topological number  $Q$  changes from  $-1$  to  $-2$  when  $J_2 \approx 0.326$ , but there is no corresponding topological phase transition occurring at this point. Topological phase transitions mostly occur on the three lowest energy bands, for the rest bands, only  $C_4, C_8$  and  $C_9$  show jumps at  $J_2 \approx 0.43$ . Since magnons follow the Bose-Einstein distribution, they prefer to stay in low energy states at low temperatures. The above fact highlights the importance of the role played by the lower energy bands.

The thermal Hall conductivity (THC) as an observable physical quantity in experiments is related to the magnon band topology [31]. The THC can be obtained as follows with the help of Berry curvature [25],

$$\kappa_{ab} = -\frac{k_B^2 T}{(2\pi)^2 \hbar} \sum_{n=1}^N \int_{\mathbf{k} \in \text{FBZ}} \left\{ c_2[\rho(E_{n,\mathbf{k}})] - \frac{\pi^2}{3} \right\} \Omega_{n,\mathbf{k}} d^2 \mathbf{k}, \quad (7)$$

where  $T$  is temperature,  $N$  is the number of sub-lattices, and  $\rho(E_{n,\mathbf{k}})$  is the Bose distribution function  $\rho(E_{n,\mathbf{k}}) = (e^{E_{n,\mathbf{k}}/k_B T} - 1)^{-1}$ . The weighting function  $c_2(x)$  is defined as  $c_2(x) = (1+x) \ln^2 \frac{1+x}{x} - \ln^2 x - 2\operatorname{Li}_2(-x)$  with the Spence function  $\operatorname{Li}_2(z) = -\int_0^z \ln(1-t)/t dt$ .

Fig. 4(d) shows temperature-dependent THC curves of representative points in different areas. At higher temperatures ( $T > 0.34$ ), THC monotonically decreases with increasing  $J_2$ . This relationship no longer exists at low temperatures. Specifically, the curves of  $J_2 = 0.5$  (which belongs to area II) and  $J_2 = 1.0$  (which belongs to area IV) both show a sign change as the temperature changes. Among them, the THC of  $J_2 = 1.0$  has a larger positive area at low temperatures. The curves of the rest parameters maintain negative values at low temperatures, and the absolute value of  $J_2 = 0.3$  (which belongs to area I) is much larger than that of  $J_2 = 0.8$  (which belongs to area III) and  $J_2 = 1.1$  (which belongs to area V).

To further clarify the differences in THC, we present the energy bands with corresponding Berry curvatures of each parameter point in Fig. 5(a)-(e). For all points, the lowest energy position is at the  $\Gamma$  point. The energy gap at the  $\Gamma$  point indicates the lack of continuous symmetry, and the gap decreases with increasing  $J_2$ . Strictly speaking, all energy bands contribute to THC at finite temperature, as shown in Eq. 7. However, as the  $c_2$  function drops quickly [10], the THC at low temperature is most related to the Berry curvature in the lowest energy regions. Fig. 5(a) shows the result when  $J_2 = 0.3$ . Due to the fact that the lowest two bands both have positive Berry curvatures near the  $\Gamma$  point, the THC has the maximum negative value at low temperatures. As shown in Fig. 5(b), although the lowest two bands have inverse Berry curvatures near the  $\Gamma$  point when  $J_2 = 0.5$ , the Berry curvatures of the lowest band make greater contributions, resulting in a totally positive THC at low temperatures. Fig. 5(c) and (d) show the results of  $J_2 = 0.8$  and  $J_2 = 1.1$  respectively. The contribution of Berry curvature to THC near the  $\Gamma$  point is almost completely canceled out, since the Berry curvatures has opposite signs and the energetic separation of the lowest two bands is very small.

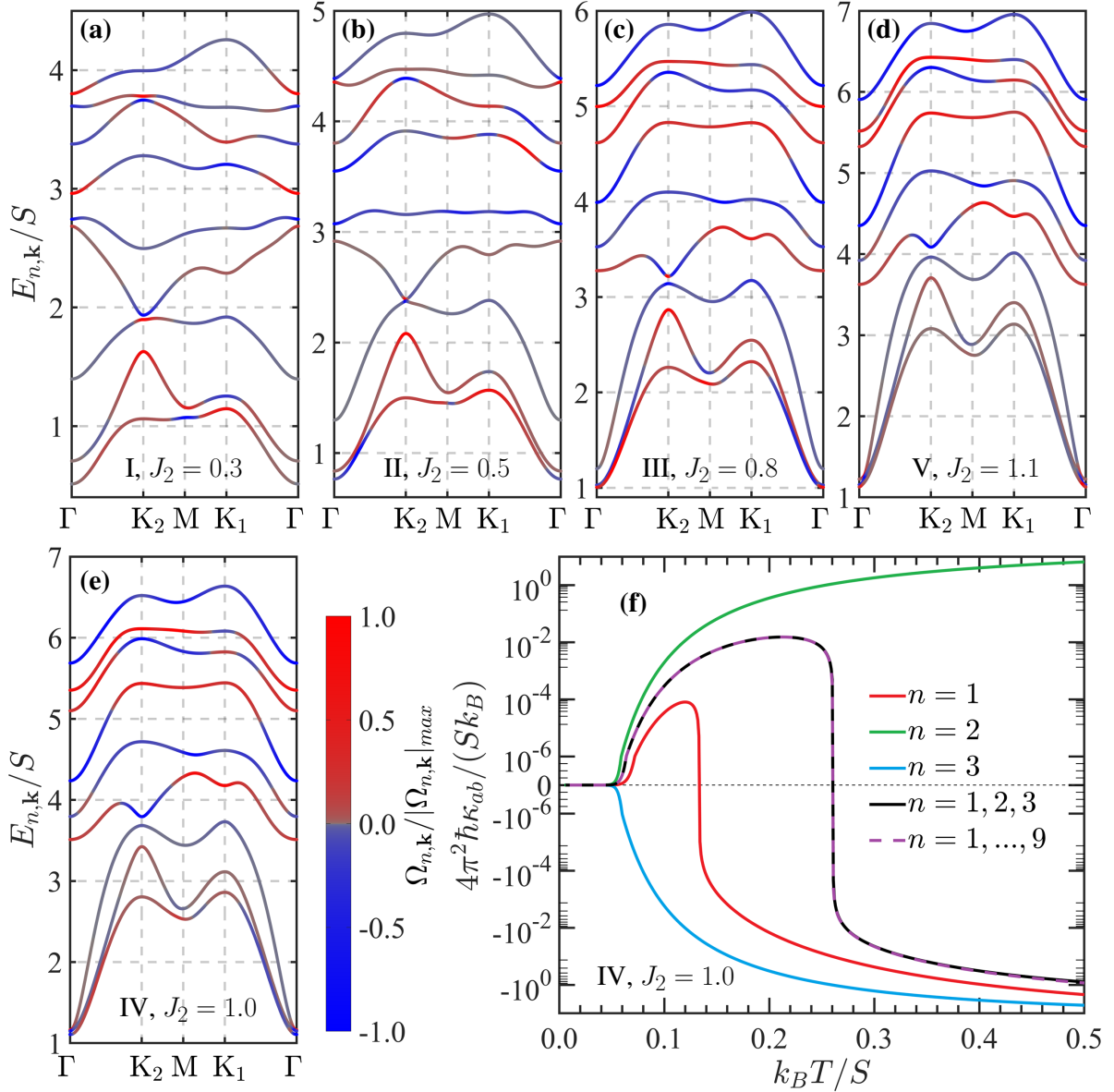


Figure 5: (a-e) Dispersion relations of different values of  $J_2$  when  $K = -1$ ,  $h = 0.05$ . They belong to different areas in Fig. 4(a) respectively. The line color stands for the normalized Berry curvature of each band. (f) The magnon thermal Hall conductivity  $\kappa_{ab}$  as a function of  $k_B T$  at the same parameter point with (e). The curves  $n = 1$ ,  $n = 2$ , and  $n = 3$  are the results coming from the single band  $n$ , and  $n = 1, 2, 3$  is the sum of them.  $n = 1, \dots, 9$  is the overall result which includes nine bands.

As shown in Fig. 5(e), when  $J_2 = 1.0$ , the position of the band with the third-lowest energy at the  $\Gamma$  point is close to the positions of bands with lower energy. To further illustrate the positive region of THC, we consider the contributions of each of the three lowest energy bands to THC separately. It can be seen in Fig. 5(f), the THC of the lowest band  $n = 1$  changes sign at  $k_B T / S \approx 0.14$ . This is because the sign of Berry curvature quickly changes from negative to positive outside the  $\Gamma$  point. The second band  $n = 2$  consistently contributes positively to THC, and the contribution of the third band  $n = 3$  to THC is always negative and cannot be neglected at low temperatures. In short, the total negative THC region stems from the combined effect of three bands. Moreover, we calculated the sum of the contributions from the lowest three bands and compared it with the total THC, and found that there is relative consistency between the two curves at low temperatures.

## 5 Summary

In summary, we found a peculiar non-coplanar order formed by the competition between bond-dependent Kitaev interaction  $K$  and next-nearest neighbor Heisenberg coupling  $J_2$  in the triangular lattice. It can be seen as a miniature version of (high-Q) skyrmion crystal since its magnetic unit cell includes nine spins and has  $\pm 1(\pm 2)$  topological number. Through the linear spin-wave theory, we studied the magnon excitations in such order. The dispersions and the corresponding Chern numbers are obtained as well. Multiple topological phases (areas) are distinguished by the Chern numbers. Of note is that the change in the relative size of  $J_2$  and  $K$  will produce topological phase transitions although the topological number in real space remains unchanged. Then we calculated the thermal Hall conductivity and discussed its differences in different areas. We found that the thermal Hall conductivity is dominated by the Berry curvature in the lowest bands at low temperatures, and in certain regions, the signs of thermal Hall conductivity will change with topological phase transitions or temperature changes. Based on these results, we hope our work will enlighten the future research of magnonics on trigonal Kitaev materials.

## Acknowledgments

We thank Xuan-yu Wang, Rui-bo Wang and Jize Zhao for their useful feedback on the manuscript. This research was supported in part by Supercomputing Center of Lanzhou University.

## A Linear spin wave theory

When considering the magnon excitations in a non-coplanar configuration with multiple spins in a magnetic unit cell, we perform the Holstein-Primakoff (HP) transformation with the quantization axis based on spin orientation. In our global coordinate system, the orientation of spin  $i$  is

$$\mathbf{S}_i = (S_i^a, S_i^b, S_i^c) = (\sin \theta_i \cos \phi_i, \sin \theta_i \sin \phi_i, \cos \theta_i). \quad (8)$$

With the help of polar angles, we can find a rotation matrix

$$R_i = \begin{bmatrix} \cos \theta_i \cos \phi_i & -\sin \phi_i & \sin \theta_i \cos \phi_i \\ \cos \theta_i \sin \phi_i & \cos \phi_i & \sin \theta_i \sin \phi_i \\ -\sin \theta_i & 0 & \cos \theta_i \end{bmatrix}, \quad (9)$$

and determine a local coordinate system  $\tilde{\mathbf{a}}\text{-}\tilde{\mathbf{b}}\text{-}\tilde{\mathbf{c}}$  that satisfying  $(S_i^a, S_i^b, S_i^c)^T = R_i (S_i^{\tilde{a}}, S_i^{\tilde{b}}, S_i^{\tilde{c}})^T$ . The spin model Eq. [1] can be rewritten as

$$\mathcal{H} = \sum_{\langle i,j \rangle, \langle\langle i,j \rangle\rangle} \mathbf{S}_i^T \cdot J_{ij} \cdot \mathbf{S}_j - \sum_i \mathbf{h} \cdot \mathbf{S}_i, \quad (10)$$

where  $J_2$  and  $K$  terms are uniformly written into the interaction matrix  $J_{ij}$ . After performing coordinate transformation on all spins separately, the model has the following form [75]

$$\mathcal{H} = \sum_{\langle i,j \rangle, \langle\langle i,j \rangle\rangle} \tilde{\mathbf{S}}_i^T R_i^T \cdot R_i \tilde{J}_{ij} R_j^T \cdot R_j \tilde{\mathbf{S}}_j - \sum_i \tilde{\mathbf{h}} R_i^T \cdot R_i \tilde{\mathbf{S}}_i. \quad (11)$$

The Holstein-Primakoff expansion [76] on spin  $i$  is

$$\begin{aligned} S_i^{\tilde{c}} &= S - b_i^\dagger b_i = S - n_i \\ S_i^{\tilde{a}} &= \frac{\sqrt{2S - n_i} b_i + b_i^\dagger \sqrt{2S - n_i}}{2} \approx \sqrt{\frac{S}{2}} (b_i + b_i^\dagger) \\ S_i^{\tilde{b}} &= \frac{\sqrt{2S - n_i} b_i - b_i^\dagger \sqrt{2S - n_i}}{2} \approx -i \sqrt{\frac{S}{2}} (b_i - b_i^\dagger), \end{aligned} \quad (12)$$



and we keep only the lowest order of the boson operator. Then we substitute  $\tilde{\mathbf{S}}_i = \left( S_i^{\bar{a}}, S_i^{\bar{b}}, S_i^{\bar{c}} \right)^T$  for each spin in a magnetic unit cell and apply the Fourier transformation

$$b_i = b_{n,j} = \frac{1}{\sqrt{L}} \sum_{\mathbf{k} \in \text{FBZ}} b_j(\mathbf{k}) e^{i\mathbf{k} \cdot (\mathbf{V}_n + \mathbf{r}_j)}, \quad (13)$$

where  $n$  is index of unit cell,  $j$  ( $\in 1, \dots, N$ ) marks the sub-lattice inside unit cell,  $L$  is the total number of unit cells and  $\mathbf{V}_n$  is Bravais lattice coordinate. Finally, we can obtain the spin wave Hamiltonian, and we focus on the quadratic term,

$$\mathcal{H}_2 = \frac{1}{2} \sum_{\mathbf{k}} \psi_{\mathbf{k}}^\dagger \mathcal{H}_{\mathbf{k}} \psi_{\mathbf{k}}, \quad (14)$$

where  $\psi_{\mathbf{k}}^\dagger = \left( a_{1,\mathbf{k}}^\dagger, a_{2,\mathbf{k}}^\dagger, \dots, a_{N,\mathbf{k}}^\dagger, a_{1,-\mathbf{k}}, a_{2,-\mathbf{k}}, \dots, a_{N,-\mathbf{k}} \right)$  and  $\mathcal{H}_{\mathbf{k}}$  is a  $2N \times 2N$  matrix. We can use a transformation matrix  $T_{\mathbf{k}}$  to diagonalize the matrix  $\mathcal{H}_{\mathbf{k}}$  [77],

$$\mathcal{E}_{\mathbf{k}} = T_{\mathbf{k}}^\dagger \mathcal{H}_{\mathbf{k}} T_{\mathbf{k}}, \quad (15)$$

where  $\mathcal{E}_{\mathbf{k}} = \text{diag} (E_{1,\mathbf{k}}, E_{2,\mathbf{k}}, \dots, E_{N,\mathbf{k}}, E_{1,-\mathbf{k}}, E_{2,-\mathbf{k}}, \dots, E_{N,-\mathbf{k}})$  contains the magnon dispersions.

## References

- [1] Bloch F 1930 *Zeitschrift für Physik* **61** 206–219 ISSN 0044-3328 URL <https://doi.org/10.1007/BF01339661>
- [2] Kubo R 1952 *Phys. Rev.* **87**(4) 568–580 URL <https://link.aps.org/doi/10.1103/PhysRev.87.568>
- [3] Dyson F J 1956 *Phys. Rev.* **102**(5) 1217–1230 URL <https://link.aps.org/doi/10.1103/PhysRev.102.1217>
- [4] Kruglyak V V, Demokritov S O and Grundler D 2010 *Journal of Physics D: Applied Physics* **43** 264001 URL <https://dx.doi.org/10.1088/0022-3727/43/26/264001>
- [5] Chumak A V, Vasyuchka V I, Serga A A and Hillebrands B 2015 *Nature Physics* **11** 453–461 ISSN 1745-2481 URL <https://doi.org/10.1038/nphys3347>
- [6] Li Z X, Cao Y and Yan P 2021 *Physics Reports* **915** 1–64 ISSN 0370-1573 URL <https://www.sciencedirect.com/science/article/pii/S0370157321000703>
- [7] Hasan M Z and Kane C L 2010 *Rev. Mod. Phys.* **82**(4) 3045–3067 URL <https://link.aps.org/doi/10.1103/RevModPhys.82.3045>
- [8] Qi X L and Zhang S C 2011 *Rev. Mod. Phys.* **83**(4) 1057–1110 URL <https://link.aps.org/doi/10.1103/RevModPhys.83.1057>
- [9] Zhang L, Ren J, Wang J S and Li B 2013 *Phys. Rev. B* **87**(14) 144101 URL <https://link.aps.org/doi/10.1103/PhysRevB.87.144101>
- [10] Mook A, Henk J and Mertig I 2014 *Phys. Rev. B* **89**(13) 134409 URL <https://link.aps.org/doi/10.1103/PhysRevB.89.134409>
- [11] Chisnell R, Helton J S, Freedman D E, Singh D K, Bewley R I, Nocera D G and Lee Y S 2015 *Phys. Rev. Lett.* **115**(14) 147201 URL <https://link.aps.org/doi/10.1103/PhysRevLett.115.147201>
- [12] Nakata K, Kim S K, Klinovaja J and Loss D 2017 *Phys. Rev. B* **96**(22) 224414 URL <https://link.aps.org/doi/10.1103/PhysRevB.96.224414>

- [13] Li B and Kovalev A A 2018 *Phys. Rev. B* **97**(17) 174413 URL <https://link.aps.org/doi/10.1103/PhysRevB.97.174413>
- [14] McClarty P A, Dong X Y, Gohlke M, Rau J G, Pollmann F, Moessner R and Penc K 2018 *Phys. Rev. B* **98**(6) 060404 URL <https://link.aps.org/doi/10.1103/PhysRevB.98.060404>
- [15] Cai Z, Bao S, Gu Z L, Gao Y P, Ma Z, Shangguan Y, Si W, Dong Z Y, Wang W, Wu Y, Lin D, Wang J, Ran K, Li S, Adroja D, Xi X, Yu S L, Wu X, Li J X and Wen J 2021 *Phys. Rev. B* **104**(2) L020402 URL <https://link.aps.org/doi/10.1103/PhysRevB.104.L020402>
- [16] Gómez Albarracín F A, Rosales H D and Pujol P 2021 *Phys. Rev. B* **103**(5) 054405 URL <https://link.aps.org/doi/10.1103/PhysRevB.103.054405>
- [17] McClarty P A 2022 *Annual Review of Condensed Matter Physics* **13** 171–190 URL <https://doi.org/10.1146/annurev-conmatphys-031620-104715>
- [18] Koyama S and Nasu J 2023 *Phys. Rev. B* **108**(23) 235162 URL <https://link.aps.org/doi/10.1103/PhysRevB.108.235162>
- [19] Matsumoto R and Murakami S 2011 *Phys. Rev. Lett.* **106**(19) 197202 URL <https://link.aps.org/doi/10.1103/PhysRevLett.106.197202>
- [20] Katsura H, Nagaosa N and Lee P A 2010 *Phys. Rev. Lett.* **104**(6) 066403 URL <https://link.aps.org/doi/10.1103/PhysRevLett.104.066403>
- [21] Onose Y, Ideue T, Katsura H, Shiomi Y, Nagaosa N and Tokura Y 2010 *Science* **329** 297–299 URL <https://www.science.org/doi/abs/10.1126/science.1188260>
- [22] Matsumoto R and Murakami S 2011 *Phys. Rev. B* **84**(18) 184406 URL <https://link.aps.org/doi/10.1103/PhysRevB.84.184406>
- [23] Ideue T, Onose Y, Katsura H, Shiomi Y, Ishiwata S, Nagaosa N and Tokura Y 2012 *Phys. Rev. B* **85**(13) 134411 URL <https://link.aps.org/doi/10.1103/PhysRevB.85.134411>
- [24] Shindou R, Matsumoto R, Murakami S and Ohe J i 2013 *Phys. Rev. B* **87**(17) 174427 URL <https://link.aps.org/doi/10.1103/PhysRevB.87.174427>
- [25] Matsumoto R, Shindou R and Murakami S 2014 *Phys. Rev. B* **89**(5) 054420 URL <https://link.aps.org/doi/10.1103/PhysRevB.89.054420>
- [26] Hirschberger M, Krizan J W, Cava R J and Ong N P 2015 *Science* **348** 106–109 URL <https://www.science.org/doi/abs/10.1126/science.1257340>
- [27] Hirschberger M, Chisnell R, Lee Y S and Ong N P 2015 *Phys. Rev. Lett.* **115**(10) 106603 URL <https://link.aps.org/doi/10.1103/PhysRevLett.115.106603>
- [28] Owerre S A 2017 *Phys. Rev. B* **95**(1) 014422 URL <https://link.aps.org/doi/10.1103/PhysRevB.95.014422>
- [29] Murakami S and Okamoto A 2017 *Journal of the Physical Society of Japan* **86** 011010 URL <https://doi.org/10.7566/JPSJ.86.011010>
- [30] Mook A, Henk J and Mertig I 2019 *Phys. Rev. B* **99**(1) 014427 URL <https://link.aps.org/doi/10.1103/PhysRevB.99.014427>
- [31] Neumann R R, Mook A, Henk J and Mertig I 2022 *Phys. Rev. Lett.* **128**(11) 117201 URL <https://link.aps.org/doi/10.1103/PhysRevLett.128.117201>
- [32] Zhuo F, Kang J, Manchon A and Cheng Z *Advanced Physics Research* 2300054 URL <https://onlinelibrary.wiley.com/doi/abs/10.1002/apxr.202300054>

- [33] Zhang X T, Gao Y H and Chen G 2023 Thermal hall effects in quantum magnets (*Preprint* 2305.04830)
- [34] Skyrme T 1962 *Nuclear Physics* **31** 556–569 ISSN 0029-5582 URL <https://www.sciencedirect.com/science/article/pii/0029558262907757>
- [35] Nagaosa N and Tokura Y 2013 *Nature Nanotechnology* **8** 899–911 ISSN 1748-3395 URL <https://doi.org/10.1038/nnano.2013.243>
- [36] Fert A, Reyren N and Cros V 2017 *Nature Reviews Materials* **2** 17031 ISSN 2058-8437 URL <https://doi.org/10.1038/natrevmats.2017.31>
- [37] Zhou Y 2018 *National Science Review* **6** 210–212 ISSN 2095-5138 URL <https://doi.org/10.1093/nsr/nwy109>
- [38] Bogdanov A N and Panagopoulos C 2020 *Nature Reviews Physics* **2** 492–498 ISSN 2522-5820 URL <https://doi.org/10.1038/s42254-020-0203-7>
- [39] Göbel B, Mertig I and Tretiakov O A 2021 *Physics Reports* **895** 1–28 ISSN 0370-1573 URL <https://www.sciencedirect.com/science/article/pii/S0370157320303525>
- [40] Yu T, Luo Z and Bauer G E 2023 *Physics Reports* **1009** 1–115 ISSN 0370-1573 URL <https://www.sciencedirect.com/science/article/pii/S0370157323000108>
- [41] Je S G, Han H S, Kim S K, Montoya S A, Chao W, Hong I S, Fullerton E E, Lee K S, Lee K J, Im M Y and Hong J I 2020 *ACS Nano* **14** 3251–3258 ISSN 1936-0851 URL <https://doi.org/10.1021/acsnano.9b08699>
- [42] Roldán-Molina A, Nunez A S and Fernández-Rossier J 2016 *New Journal of Physics* **18** 045015 URL <https://dx.doi.org/10.1088/1367-2630/18/4/045015>
- [43] Díaz S A, Klinovaja J and Loss D 2019 *Phys. Rev. Lett.* **122**(18) 187203 URL <https://link.aps.org/doi/10.1103/PhysRevLett.122.187203>
- [44] Díaz S A, Hiroswawa T, Klinovaja J and Loss D 2020 *Phys. Rev. Res.* **2**(1) 013231 URL <https://link.aps.org/doi/10.1103/PhysRevResearch.2.013231>
- [45] Mæland K and Sudbø A 2022 *Phys. Rev. Res.* **4**(3) L032025 URL <https://link.aps.org/doi/10.1103/PhysRevResearch.4.L032025>
- [46] Timofeev V E and Aristov D N 2022 *Phys. Rev. B* **105**(2) 024422 URL <https://link.aps.org/doi/10.1103/PhysRevB.105.024422>
- [47] Akazawa M, Lee H Y, Takeda H, Fujima Y, Tokunaga Y, Arima T h, Han J H and Yamashita M 2022 *Phys. Rev. Res.* **4**(4) 043085 URL <https://link.aps.org/doi/10.1103/PhysRevResearch.4.043085>
- [48] Weber T, Fobes D M, Waizner J, Steffens P, Tucker G S, Böhm M, Beddrich L, Franz C, Gabold H, Bewley R, Voneshen D, Skoulatos M, Georgii R, Ehlers G, Bauer A, Pfeiderer C, Böni P, Janoschek M and Garst M 2022 *Science* **375** 1025–1030 URL <https://www.science.org/doi/abs/10.1126/science.abe4441>
- [49] Okubo T, Chung S and Kawamura H 2012 *Phys. Rev. Lett.* **108**(1) 017206 URL <https://link.aps.org/doi/10.1103/PhysRevLett.108.017206>
- [50] Utesov O I 2021 *Phys. Rev. B* **103**(6) 064414 URL <https://link.aps.org/doi/10.1103/PhysRevB.103.064414>
- [51] Leonov A O and Mostovoy M 2015 *Nature Communications* **6** 8275 ISSN 2041-1723 URL <https://doi.org/10.1038/ncomms9275>

- [52] Hayami S, Lin S Z and Batista C D 2016 *Phys. Rev. B* **93**(18) 184413 URL <https://link.aps.org/doi/10.1103/PhysRevB.93.184413>
- [53] Lin S Z and Batista C D 2018 *Phys. Rev. Lett.* **120**(7) 077202 URL <https://link.aps.org/doi/10.1103/PhysRevLett.120.077202>
- [54] Amoroso D, Barone P and Picozzi S 2020 *Nature Communications* **11** 5784 ISSN 2041-1723 URL <https://doi.org/10.1038/s41467-020-19535-w>
- [55] Hayami S 2021 *Phys. Rev. B* **103**(22) 224418 URL <https://link.aps.org/doi/10.1103/PhysRevB.103.224418>
- [56] Wang Z, Su Y, Lin S Z and Batista C D 2021 *Phys. Rev. B* **103**(10) 104408 URL <https://link.aps.org/doi/10.1103/PhysRevB.103.104408>
- [57] Hirschberger M, Hayami S and Tokura Y 2021 *New Journal of Physics* **23** 023039 URL <https://dx.doi.org/10.1088/1367-2630/abdef9>
- [58] Utesov O I 2022 *Phys. Rev. B* **105**(5) 054435 URL <https://link.aps.org/doi/10.1103/PhysRevB.105.054435>
- [59] Hayami S 2022 *Journal of Magnetism and Magnetic Materials* **564** 170036 ISSN 0304-8853 URL <https://www.sciencedirect.com/science/article/pii/S0304885322009210>
- [60] Hayami S 2023 *Anisotropic skyrmion crystal on a centrosymmetric square lattice under an in-plane magnetic field* arXiv:2312.01542 URL <https://arxiv.org/abs/2312.01542>
- [61] Yao X and Dong S 2016 *Scientific Reports* **6** 26750 ISSN 2045-2322 URL <https://doi.org/10.1038/srep26750>
- [62] Rousochatzakis I, Rössler U K, van den Brink J and Daghofer M 2016 *Phys. Rev. B* **93**(10) 104417 URL <https://link.aps.org/doi/10.1103/PhysRevB.93.104417>
- [63] Chen K, Luo Q, Zhou Z, He S, Xi B, Jia C, Luo H G and Zhao J 2023 *New Journal of Physics* **25** 023006 URL <https://dx.doi.org/10.1088/1367-2630/acb5bb>
- [64] Winter S M, Tsirlin A A, Daghofer M, van den Brink J, Singh Y, Gegenwart P and Valentí R 2017 *Journal of Physics: Condensed Matter* **29** 493002 URL <https://dx.doi.org/10.1088/1361-648X/aa8cf5>
- [65] Trebst S and Hickey C 2022 *Physics Reports* **950** 1–37 ISSN 0370-1573 URL <https://www.sciencedirect.com/science/article/pii/S0370157321004051>
- [66] Razpopov A, Kaib D A S, Backes S, Balents L, Wilson S D, Ferrari F, Riedl K and Valentí R 2023 *npj Quantum Materials* **8** 36 ISSN 2397-4648 URL <https://doi.org/10.1038/s41535-023-00567-6>
- [67] Aoyama K and Kawamura H 2022 *Phys. Rev. B* **105**(10) L100407 URL <https://link.aps.org/doi/10.1103/PhysRevB.105.L100407>
- [68] Kim C, Kim S, Park P, Kim T, Jeong J, Ohira-Kawamura S, Murai N, Nakajima K, Chernyshev A L, Mourigal M, Kim S J and Park J G 2023 *Nature Physics* **19** 1624–1629 ISSN 1745-2481 URL <https://doi.org/10.1038/s41567-023-02180-7>
- [69] Hukushima K and Nemoto K 1996 *Journal of the Physical Society of Japan* **65** 1604–1608 ISSN 1347-4073 URL <http://dx.doi.org/10.1143/JPSJ.65.1604>
- [70] Miyatake Y, Yamamoto M, Kim J J, Toyonaga M and Nagai O 1986 *Journal of Physics C: Solid State Physics* **19** 2539 URL <https://dx.doi.org/10.1088/0022-3719/19/14/020>

- [71] Janssen L, Andrade E C and Vojta M 2016 *Phys. Rev. Lett.* **117**(27) 277202 URL <https://link.aps.org/doi/10.1103/PhysRevLett.117.277202>
- [72] Shimokawa T, Okubo T and Kawamura H 2019 *Phys. Rev. B* **100**(22) 224404 URL <https://link.aps.org/doi/10.1103/PhysRevB.100.224404>
- [73] Berg B and Lüscher M 1981 *Nuclear Physics B* **190** 412–424 ISSN 0550-3213 URL <https://www.sciencedirect.com/science/article/pii/055032138190568X>
- [74] Becker M, Hermanns M, Bauer B, Garst M and Trebst S 2015 *Phys. Rev. B* **91**(15) 155135 URL <https://link.aps.org/doi/10.1103/PhysRevB.91.155135>
- [75] Zhang E Z, Chern L E and Kim Y B 2021 *Phys. Rev. B* **103**(17) 174402 URL <https://link.aps.org/doi/10.1103/PhysRevB.103.174402>
- [76] Holstein T and Primakoff H 1940 *Phys. Rev.* **58**(12) 1098–1113 URL <https://link.aps.org/doi/10.1103/PhysRev.58.1098>
- [77] Colpa J 1978 *Physica A: Statistical Mechanics and its Applications* **93** 327–353 ISSN 0378-4371 URL <https://www.sciencedirect.com/science/article/pii/0378437178901607>